Title
Senescent changes in photopic spatial summation in the peripheral retina

Journal
PERCEPTION, 38

ISSN
0301-0066

Authors
Malania, M
Werner, JS

Publication Date
2009

Peer reviewed

Senescent changes in photopic spatial summation

Maka Malania — Department of Ophthalmology and Vision Science, University of California, Davis, USA

Frédéric Devinck — Laboratoire de Psychologie Expérimentale (E.A. 1285), Université de Rennes 2, Rennes, France

Kenneth Knoblauch — INSERM, U846, Stem-cell and Brain Research Institute, Department of Integrative Neurosciences, Bron, France, & Université de Lyon, Lyon, France

Peter B. Delahunt — Posit Science Corporation, San Francisco, CA, USA

Joseph L. Hardy — Lumos Labs, Incorporated, San Francisco, CA, USA

John S. Werner — Department of Ophthalmology and Vision Science, University of California, Davis, USA

Previous studies have demonstrated an inverse relation between the size of the complete spatial summation area and ganglion cell density. We hypothesized that if this relation is dynamic, the spatial summation area at 6° nasal would expand to compensate for age-related losses of retinal ganglion cells but not in the fovea where age-related loss in ganglion cell density is not significant. This hypothesis was tested by measuring contrast thresholds with a series of Gabor patches varying in size. The spatial summation area was defined by the intersection of the segments of a two-branched, piece-wise linear function fitted to the data with slopes of −0.5 and 0 on a plot of log threshold vs. log area. Results demonstrate a 31% increase in the parafoveal spatial summation area in older observers with no significant age-related change in the fovea. The average foveal data show a significant increase in thresholds with age. Contrary to the foveal data, age comparisons of the parafoveal peak contrast thresholds display no significant difference above the summation area. Nevertheless, as expected from the increase in summation area, expressing the parafoveal thresholds as contrast energy reveals a significant difference for stimuli that are smaller than the maximal summation area.

Keywords: spatial summation, human aging, contrast sensitivity, ganglion cells

Citation: Malania, M., Devinck, F., Knoblauch, K., Delahunt, P. B., Hardy, J. L., & Werner, J. S. (2011). Senescent changes in photopic spatial summation. *Journal of Vision, 11*(10):15, 1–15, http://www.journalofvision.org/content/11/10/15, doi:10.1167/11.10.15.

Introduction

The sampling limits of the human visual system depend upon optical and neural factors, both of which change across the life span (Werner, Schefrin, & Bradley, 2010). These senescent changes provide a probe into possible dynamic modifications that support vision in elderly observers, notwithstanding inevitable age-related losses in vision even in the absence of age-related disease.

Classically, spatial integration has been quantified from measurements of thresholds for a series of small test stimuli. Over small regions, these thresholds depend on a constant amount of energy regardless of its spatial distribution. Therefore, over a restricted region of the visual field, the energy required for threshold and stimulus area is reciprocally related. The largest area over which this relation obtains is known as the complete summation area or Ricco's (1877) area in honor of the Italian astronomer who described this as the "Law of Compensation." Ricco's law is valid for relatively small stimuli, ranging from 2 arcmin in the fovea at photopic luminances to 1 deg in the periphery (Graham & Margaria, 1935; Scholtes & Bouman, 1977) depending on the stimulus conditions. For medium stimulus sizes, and when using gratings, thresholds typically decrease in proportion to the square root of stimulus area, following Piper's (1903) law. Figure 1 (solid lines) illustrates a typical two-branched, piece-wise linear summation curve. The upper branch of the curve has a slope of −0.5, which is followed by a size-independent region having a slope of 0. Whether one observes Ricco's law, Piper's law, or both before reaching the size-independent region depends on numerous parameters (Barlow, 1958; Cohn, 1990; Sakitt, 1971). Here, we tested sensitivity using a series of Gabor patches, so the primary interest is the intersection of the descending function (slope of −0.5 for our conditions) and the size-independent area, which we define as the spatial summation area.

doi: 10.1167/11.10.15 Received September 26, 2010; published September 22, 2011 ISSN 1534-7362

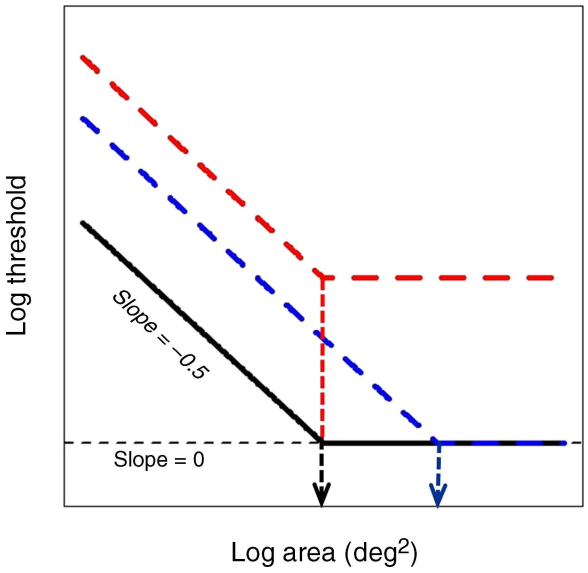

Figure 1. Model for spatial summation in which log threshold (I) decreases with stimulus area (A). In this example, the first branch (slope = −0.5) follows Piper's law, Constant = $I * A^{1/2}$, and the second branch (slope = 0) is independent of area. The spatial summation area is defined here by the stimulus area at the intersection of the two branches (denoted by an arrow). The red-dashed piece-wise linear function shows the expected effect of age-related changes only due to an increased threshold relative to a younger observer, denoted by the black piece-wise linear function. The blue-dashed piece-wise linear function shows the effect on thresholds of an increase in the spatial summation area with no concomitant vertical shift of the data, i.e., only a lateral shift of the curve.

Areal summation has been demonstrated under both photopic and scotopic conditions (Barlow, 1958; Glezer, 1965; Wilson, 1970). In the central fovea, the size of the complete summation area is on the order of a single cone diameter presumably due to the lack of convergence onto bipolar and ganglion cells. Diffraction and aberrations (Davila & Geisler, 1991), causing the light to be imaged over an area of more than one cone photoreceptor, however, may influence psychophysical estimates of spatial summation. Outside the fovea, the size of spatial summation areas has been explained by ganglion cell sampling density (Lie, 1980) and receptive field center size (Glezer, 1965; Inui, Mimura, & Kani, 1981; Richards, 1967). Fischer (1973) proposed that the change in the size of the spatial summation area with retinal eccentricity is determined by stimulation of a constant number of ganglion cells. Thus, the size of the summation area increases with lower ganglion cell sampling density at greater retinal eccentricity. Stimulating a constant number of ganglion cells is equivalent to activating a constant amount of cortical area V1 (Rovamo, Virsu, & Näsänen, 1978). This idea is consistent with evidence from Ransom-Hogg and Spillmann (1980) that a constant amount of cortical space, based on ganglion cell field density (ganglion cell density corrected for cell bodies displaced from the fovea), subserves a perceptive field.

There are numerous age-related changes in the eye and retina that could affect spatial summation curves. Reduced transmission of the ocular media (van der Kraats & van Norren, 2007; Weale, 1988), increases in light scatter (Allen & Vos, 1967; Wolf & Gardner, 1965), reduced pupil size (Winn, Whitaker, Elliott, & Phillips, 1994), reductions in rod (Jackson & Owsley, 2000; Schefrin, Bieber, McLean, & Werner, 1998) and cone sensitivity (Werner, Schefrin, & Bieber, 2000), losses in cone and rod numbers (Curcio, Millican, Allen, & Kalina, 1993; Panda-Jonas, Jonas, & Jakobczyk-Zmija, 1995), or changes in receptor efficiency (Werner, Schelble, & Bieber, 2001) would cause an increase in thresholds, thereby elevating the two-branched summation function as shown in Figure 1 (red, dashed lines). By themselves, these changes would not, however, be expected to result in changes in the spatial summation area. Additional age-related changes such as losses in ganglion cell density (Curcio & Allen, 1990; Curcio & Drucker, 1993; Harman, Abrahams, Moore, & Hoskins, 2000; Morrison, Cork, Dunkelberger, Brown, & Quigley, 1990; Quigley, Dunkelberger, & Green, 1989) and subsequent rewiring of neural circuitry would be expected to lead to an increase in the size of the spatial summation area as illustrated by the lateral shift of the summation area in Figure 1 denoted by the blue, dashed function.

Anatomical and morphological studies show age-related losses in rod photoreceptors, but surviving rods enlarge so that there are no gaps in the retinal mosaic at the level of the inner segments (Curcio, Medeiros, & Millican, 1998). This result suggests that there may be structural changes that compensate for age-related losses at a cellular level. To evaluate the functional correlates of monotonic loss of rod photoreceptors and ganglion cells over the adult life span, Schefrin et al. (1998) measured scotopic spatial summation in 50 observers ranging from 19 to 87 years of age. They found that the area of complete scotopic spatial summation increased by ~55% between the ages of 34 and 71 years. These ages were chosen for comparison with Curcio's ganglion cell counts, corrected for their displacement from the photoreceptor area that they subserve. Modeling of these data showed that changes in spatial summation cannot be explained by age-related changes in the modulation transfer function (Artal, Ferro, Miranda, & Navarro, 1993) or light scatter (Liang & Westheimer, 1995). One possible explanation is that there are selective age-related losses of sensitivity to relatively high spatial frequencies causing detection to be based on low spatial frequency-tuned neurons, but this hypothesis was rejected based on subsequent measures of the scotopic contrast sensitivity function (Schefrin, Tregear, Harvey, & Werner, 1999). Schefrin, Hauser, and Werner (2004) later tested psychophysically the hypothesis that ganglion cell receptive fields increase in size with age perhaps due to

reorganization at postreceptoral levels following rod losses and the sprouting of rod neurites that occurs among surviving rods in response to the death of their neighbors (Li, Kljavin, & Milam, 1995; Milam, Li, & Fariss, 1998). This hypothesis was rejected, as might have been expected from single-unit responses of LGN cells in old monkeys (Spear, 1993). Another possible site of synaptic reorganization is at the level of the visual cortex, as at any given eccentricity the spatial summation area is likely subserved by a constant afferent input to the cortex (Fischer, 1973; Ransom-Hogg & Spillmann, 1980; Volbrecht, Shrago, Schefrin, & Werner, 2000). Remarkably, the age-related enlargement of the spatial summation area is related to the reduction in ganglion cell density over the same age range (Curcio & Drucker, 1993). This implies that the number of ganglion cells subserving the spatial summation area is constant across age. However, in order to maintain this constancy, some of the ganglion cells subserving a particular summation area must change with age. One explanation for these results is that cortical cells that have lost their primary afferent input now receive input from neighboring cortical cells through gating of lateral connections, thereby causing a reorganization in cortical mapping (Gilbert & Wiesel, 1992; Merzenich et al., 1984).

Two recent studies have examined photopic spatial summation functions in relation to normal aging and glaucoma (Redmond, Garway-Heath, Zlatkova, & Anderson, 2010; Redmond, Zlatkova, Garway-Heath, & Anderson, 2010). Ganglion cell density was inferred from an achromatic peripheral grating resolution task (Thibos, 1998). This measure was uncorrelated with the transition between slopes of −1 and −0.5 as a function of age, but the transition did occur at larger stimulus areas in glaucoma patients compared to normal controls. It is known that glaucoma is characterized by substantial loss of ganglion cells. These authors concluded from the glaucoma patients that an enlargement of the summation area may compensate for sensitivity losses that would otherwise occur with reduced ganglion cell sampling. This result supported findings by Schefrin et al. (1998) that the size of the spatial summation area is defined by the density of ganglion cells.

The purpose of the present study was to test the hypothesis that there is selective enlargement of the photopic spatial summation area, based on the hypothesis that age-related reorganization of spatial vision follows loss of ganglion cells. To that end, we compared two retinal areas that anatomical studies have shown to differ with respect to age-related loss of ganglion cells. Spatial summation was defined in terms of contrast sensitivity with Gabor patches of increasing area. A number of studies have shown that contrast sensitivity increases with the number of grating cycles or stimulus area up to a critical size (Hoekstra, van der Goot, van den Brink, & Bilsen, 1974; Howell & Hess, 1978; Rovamo, Luntinen, & Näsänen, 1993; Savoy & McCann, 1975). In this study, a vertical Gabor was used to target spatiotemporal filters that underlie early cortical processing (Daugman, 1985; Jones & Palmer, 1987).

General methods

Observers

Foveal spatial summation was measured for 10 younger (19–23 years, mean age of 21 years) and 10 older (67–83 years, mean age of 74 years) healthy observers, divided equally between males and females. The same older observers participated in the measurement of parafoveal spatial summation, while three younger observers were different for the parafoveal measurements (resulting in 3 females and 7 males). Ancillary analyses (*t*-tests) of the seven observers who completed all measurements revealed no significant differences ($p > 0.05$) from those reported for the complete samples.

All subjects had normal or corrected-to-normal visual acuity and were free from any ocular or neurological disease. The mean refractive error for the younger group was −1.66 ± 1.40 diopter (D) sphere and +0.2 ± 0.22 D cylinder, and for older observers, it was +0.34 ± 1.29 D sphere and +0.91 ± 0.81 D cylinder. The best corrected mean log MAR was −0.077 (range = 0 to −0.125) for younger subjects and −0.003 (range = 0.097 to −0.125) for older subjects. Observers were carefully screened for the presence of abnormal ocular media and retinal disease based upon slit lamp examination, as well as direct and indirect ophthalmoscopy. Fundus photos were reviewed by a retinal specialist. All subjects demonstrated normal color vision when tested with the Farnsworth Panel D-15 test, the F-2 plate, and American Optical HRR pseudoisochromatic plates. Subjects were refracted for the test distance. Written informed consent was obtained from all participants, and all experimental protocols were approved by the Institutional Review Board of the University of California, Davis, School of Medicine and in accordance with the principles of the Declaration of Helsinki.

Stimuli and procedure

Stimuli were presented on a CRT monitor (Sony Trinitron) driven by a 10-bit graphics card in a Macintosh G4 computer using the OS9 operating system. Screen resolution was 1792 × 1344 pixels (1-degree diameter contained 47 pixels) and had a refresh rate of 75 Hz. Calibration was performed with a Minolta colorimeter (CS 100 Chroma Meter) following procedures described by Brainard, Pelli, and Robson (2002), and lookup tables were used to enable a linear manipulation of screen luminance. The experimental software was written in MATLAB (version 5.2, MathWorks) using the Psychophysics Toolbox

extensions (Brainard, 1997; Pelli, 1997). The monitor was imaged on the retina by a Maxwellian-view optical system with a 2.2-mm diameter exit pupil to control for age-related variations in pupil size. Thus, we were able to maintain constant retinal illumination at ~78 Td for all observers. Head position was stabilized with a bite bar, and an auxiliary optical system was used to align the eye pupil to the optic axis of the Maxwellian-view system. The stimuli were viewed monocularly, using the eye with superior visual acuity or by individual preference, with the other eye patched. Before testing, each observer had one or more practice sessions. The observers participated in the experiments over multiple days of testing for 1–2 h per day.

The experiments took place in a dark room after a minimum of 5 min of dark adaptation followed by 1–2 min adaptation to a blank screen at the luminance of the test stimuli. Stimuli were vertical sinusoidal gratings tapered by a two-dimensional Gaussian envelope (σ = stimulus size / 4) in sine-wave phase. The sinusoidal grating was modulated in counterphase (light–dark reversal) at a reversal rate of 0.5 cycle/s. All stimuli were achromatic with a chromaticity of CIE Illuminant C (CIE x, y = 0.310, 0.316). The stimuli were presented on a background of the same mean luminance and chromaticity. Stimulus contrast was defined as the Michelson contrast of the sine-wave component, $(L_{max} - L_{min}) / (L_{max} + L_{min})$, where L_{max} is the maximal luminance and L_{min} is the minimal luminance in the sine wave. We manipulated the stimulus size, varying it in area from 0.24 to 28.26 deg^2 (diameters: 0.55 to 6.00 deg), while keeping the spatial frequency constant. Stimulus duration was 750 ms with 500-ms interstimulus intervals. Each stimulus size was tested in separate blocks, and observers were aware of which stimulus was being used as a target. A temporal two-alternative forced-choice (2-AFC) task, controlled by an adaptive staircase procedure, QUEST (Watson & Pelli, 1983), was used to obtain contrast detection thresholds. For each test session, data were collapsed across the two randomly interleaved staircases. The QUEST procedure terminated if the standard deviation of the threshold estimate dropped below 0.05 log unit of contrast after a minimum of 45 trials (per staircase) or if both staircases reached 100 trials. The observer's task was to detect the interval containing the stimulus and respond by pushing a button. The order of the signal and blank intervals was randomized. An auditory signal denoted the beginning of each stimulus interval. Observers were instructed to fixate the center of the test screen. A dark fixation point appeared on the screen before the start of each trial. It was displayed on the screen continuously during parafoveal stimulus presentations.

Two conditions were tested. In the first experiment, we measured contrast detection thresholds for the patterns centered on the fovea having a spatial frequency of 5 cycles per degree (cpd). In the second set of experiments, contrast detection thresholds were measured for a pattern presented at 6-degree nasal retina, with a spatial frequency of 4 cpd. The number of cycles per sigma ranged from 0.56 to 6 for 4-cpd stimuli and from 0.7 to 7.5 for 5-cpd stimuli. These spatial frequencies were chosen after extensive pilot testing, based on the sizes of the spatial summation areas and age-related differences in contrast sensitivity functions. These stimuli are near or above the high-frequency cutoff for scotopic contrast sensitivity reported for younger (Lennie & Fairchild, 1994) and older (Schefrin et al., 1999) observers. Using Gabor stimuli has the advantage that the spatial Gaussian weighted envelope reduces the effect of spatial nonuniformity by localizing the stimuli to a small region in both the space and frequency domains (Graham, Robson, & Nachmias, 1978). It has been shown that the spatial sensitivity functions of V1 neurons in monkeys have a form similar to two-dimensional Gabor functions (Marcelja, 1980; Ringach, 2002).

Results

Comparison of foveal and parafoveal data sets

Contrast detection thresholds plotted as a function of stimulus area for the foveal data are shown for individual observers in separate panels of Figure 2 and for the parafoveal data in Figure 4. The parafoveal data were collected at 6 deg in the nasal retina, an area associated with age-related loss in retinal ganglion cells (Harman et al., 2000). Figures 3 and 5 show the average data sets obtained in the fovea and parafovea, respectively. The error bars are 95% confidence intervals for interobserver differences. The average foveal data display a systematic increase in threshold with age, but evidence for a difference in the lateral positions of the curves is less obvious. In the parafovea, the older observers display higher thresholds on average than the younger observers, but the thresholds are much more similar beyond the summation region. The areal summation limit for the older observers is shifted laterally to larger areas, in contrast to the average shift in the foveal data.

Initially, we analyzed the effects of age and area using a linear mixed-effects model (Bates, Maechler, & Bolker, 2011; Pinheiro & Bates, 2000) at each eccentricity, separately. The response or dependent variable was the logarithm of the threshold contrast. Age and area were treated as factors and taken as fixed effects. Observer and area within observer were treated as random effects. The random effect of area within observer is the variability from repeated estimation of threshold for an observer at a given area. We will refer to these as between and within effects because they correspond to between observer and within observer and areal sources of variability, respectively. We fit and tested three nested models of increasing complexity including: (1) a main effect of area, (2) main effects of area and age, and (3) main effects

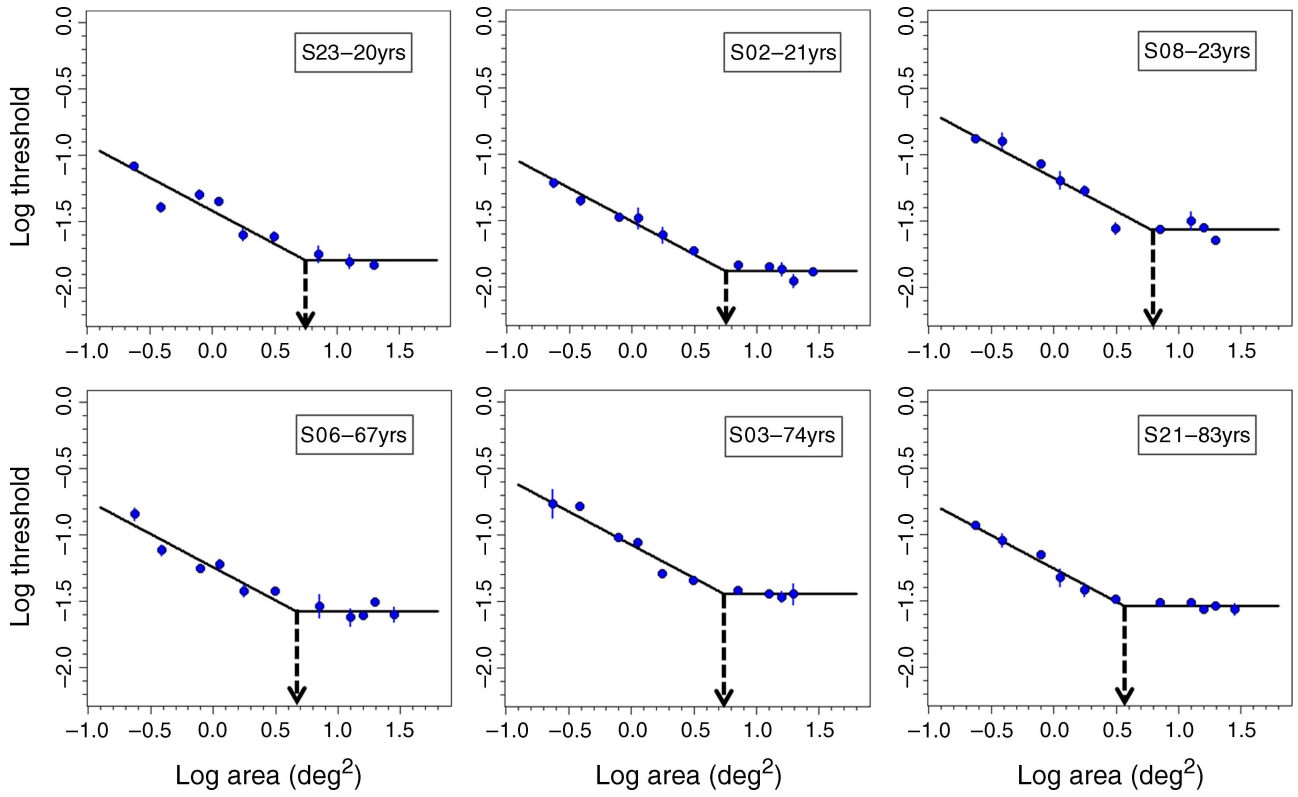

Figure 2. Foveal log contrast detection thresholds (±1 *SEM*) plotted as a function of log stimulus area. Smooth functions show model fits using Equation 1. The inflection point of fitted functions defines the spatial summation area (A_{max}) marked by the arrows in each plot. The identification code and the age of individual observers are shown in the upper right of each plot.

of both factors and their interaction. Successive comparisons between the models were performed with likelihood ratio tests, the results of which are summarized in Tables 1 (fovea) and 2 (parafovea).

For the foveal data, adding a fixed-effect of age led to a significant improvement in the model fit but not the addition of the interaction of age and area. Given the average data in Figure 3, this indicates that older observers are less sensitive than younger observers, but the difference in the lateral positions of the summation curves is not significant.

For the parafoveal data, the interaction term is significant, consistent with the above observation that the data sets display both vertical and lateral shifts. The presence of the interaction renders it difficult to interpret directly a main effect of age because the size of the effect depends on the stimulus area. Therefore, we will turn to a curve-fitting approach in the next two sections to obtain separate estimates of the vertical and lateral shifts in the data.

We report the square roots of the estimated variance components for the best fitting models because they are in the same units as the dependent variable. The square root of the between variance was 0.178 in the foveal and 0.199 in the parafoveal data. For the within component, the estimates were 0.067 in the fovea and 0.057 in the parafovea. The square root of the residual variance was 0.066 in the fovea and 0.067 in the parafovea. The ratio of between to

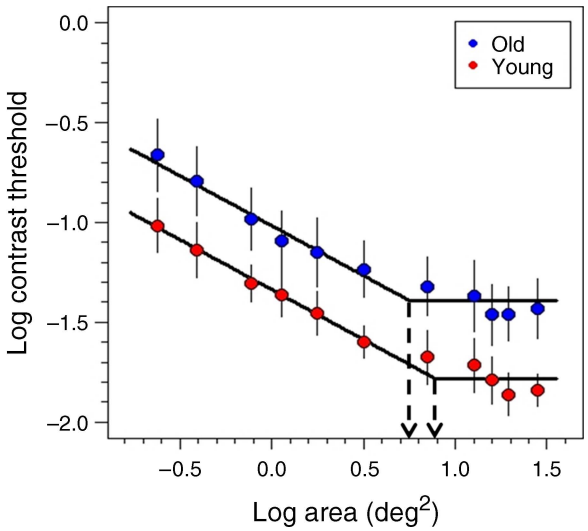

Figure 3. Mean log thresholds versus log area for stimuli presented at the fovea. Symbols denote the mean data for the younger (red) and older (blue) observers. The error bars are 95% confidence intervals for interobserver differences. The parameters of the best fitting model (Equation 2) to the mean log threshold were used for the curves.

Model	*df*	Log likelihood	χ^2	Δdf	Pr(>χ^2)
Area	14	378.45			
Area + Age	15	385.56	14.21	1	2.00e − 04
Area + Age + Age:Area	25	393.81	16.5	10	0.086

Table 1. Summary of the fits of three nested mixed-effects models to the foveal data and likelihood ratio tests. Column 1: Model terms. Column 2: Degrees of freedom of the model. Column 3: Logarithm of the likelihood. Column 4: χ^2 statistic for the successive differences between the models. Column 5: Difference in degrees of freedom between the models. Column 6: *p*-value for the observed χ^2 statistic.

within components is approximately a factor of three. The similarity of estimates in the foveal and parafoveal data sets indicates similar contributions of each variance source at each eccentricity and suggests that the goodness of fits were similar.

Foveal spatial summation

To evaluate the differences between the data sets of young and old observers in the fovea and parafovea, we used a curve-fitting approach to estimate parameters corresponding to their sensitivity and summation characteristics. We consider the foveal data in this section and the parafoveal data in the next. Data were fit with a function containing two linear segments such that

$$\begin{aligned} \log(\mathrm{TC}) &= k - 0.5(\log(A) - \log(A_{\max})), & A \le A_{\max} \\ &= k, & A > A_{\max}, \end{aligned} \quad (1)$$

where TC is the threshold contrast, A is the stimulus area, and k and $A_{\max}$ are estimated parameters. The first segment has a slope of -0.5 and the second a slope of 0 at an ordinate value given by k. The two segments intersect at the abscissa value of $A_{\max}$, which corresponds to the maximal area showing square root summation. The two parameters k and $A_{\max}$ control, respectively, the vertical and horizontal positions of the function. While each segment is linear, the problem requires a nonlinear regression because parameter $A_{\max}$ must also be estimated. Equation 1 can be parameterized in a single equation as follows:

$$\log(\mathrm{TC}) = \beta(|\log(A) - \log(A_{\max})| - \log(A) + \log(A_{\max})) + k, \quad (2)$$

where $\beta = 0.25$ yields the same behavior as Equation 1. Equation 2 was fit to each observer's data initially with 3 parameters (β, $A_{\max}$, k) and subsequently with only two parameters with $\beta = 0.25$. Parameter estimation was based on a least-squares criterion using a Gauss–Newton algorithm to search for the best fit. All calculations and statistical tests were done within R (R Development Core Team, 2010).

The two-parameter model is nested in the three-parameter model, so we can compare them using a likelihood ratio test. Sixteen of the 20 fits yielded no significant difference for $p > 0.05$ (18 for $p > 0.01$), and this number increased to 18 after adjusting for multiple testing using Bonferroni's correction. The parameter estimates and summary information of the fits of the two-parameter model for each observer are shown in Table 3. The approximate standard errors for each parameter estimate (columns 3 and 5) are based on the square root of the diagonal of the variance–covariance matrix. The residual standard error of the fit (column 7) is the square root of the sum of squared residuals (column 6) divided by the square root of degrees of freedom (the number of points minus the number of estimated parameters). The fits of the two-parameter model to individual observer's data are shown as the solid lines in Figure 2 for representative observers, and fits based on the average parameters for 10 younger and 10 older observers are shown in Figure 3. Arrows point to the spatial summation areas defined by the intersection of the two-segmented function. In units of diameter, these points correspond to 3.16 and 2.67 deg, in the younger and older groups, respectively.

We evaluated the effect of age for each of the parameters, using Student's *t*-tests. As suggested by the mixed-effects models in the previous section, the difference in summation area, $\log_{10}A_{\max}$, is not significant ($t = 1.228$, $df = 18$,

Model	*df*	Log likelihood	χ^2	Δdf	Pr(>χ^2)
Area	14	415.08			
Area + Age	15	417.44	4.72	1	0.03
Area + Age + Age:Area	25	433.41	31.94	10	4.00e − 04

Table 2. Summary of the fits of three nested mixed-effects models to the parafoveal data and likelihood ratio tests. Column 1: Model terms. Column 2: Degrees of freedom. Column 3: Logarithm of the likelihood. Column 4: χ^2 statistic for the successive differences between the models. Column 5: Difference in degrees of freedom between the models. Column 6: *p*-value for the observed χ^2 statistic.

Observer ID number	$\log_{10} A_{max}$	Standard error ($\log_{10} A_{max}$)	k	Standard error (k)	Residual SSE	Residual standard error	Age (years)
S02	0.748	0.073	−1.878	0.027	0.071	0.06	21
S05	0.682	0.098	−1.793	0.042	0.038	0.052	23
S07	0.764	0.073	−1.57	0.027	0.17	0.092	21
S08	0.893	0.075	−1.615	0.03	0.17	0.092	23
S10	0.982	0.075	−1.901	0.03	0.09	0.067	21
S15	1.367	0.126	−1.937	0.06	0.117	0.076	21
S16	0.923	0.083	−1.983	0.035	0.088	0.07	21
S17	0.408	0.087	−1.428	0.035	0.195	0.118	21
S19	1.363	0.126	−1.905	0.06	0.238	0.109	19
S23	0.817	0.085	−1.825	0.035	0.174	0.104	20
S03	0.742	0.077	−1.443	0.03	0.079	0.066	74
S06	0.666	0.073	−1.575	0.027	0.123	0.078	67
S09	0.313	0.087	−0.958	0.035	0.238	0.13	70
S11	1.234	0.094	−1.625	0.042	0.146	0.085	67
S12	0.655	0.077	−1.191	0.03	0.086	0.069	83
S13	0.766	0.077	−1.782	0.03	0.205	0.107	68
S14	0.955	0.075	−1.331	0.03	0.123	0.079	77
S20	0.758	0.073	−1.207	0.027	0.127	0.08	80
S21	0.569	0.073	−1.538	0.027	0.043	0.046	83
S22	0.813	0.073	−1.246	0.027	0.133	0.081	72

Table 3. Summary of the fits of the 2-parameter model to the foveal data for each observer. Column 1: Observers' unique identification number. Column 2: $\log_{10} A_{max}$ estimate. Column 3: Standard error of $\log_{10} A_{max}$. Column 4: k estimate. Column 5: Standard error of k. Column 6: Residual sum of squared error. Column 7: Residual standard error of the fit. Column 8: Age of observers.

$p = 0.24$), but the difference in heights of the curves as indexed by parameter k is significant ($t = -4.043$, $df = 18$, $p = 8e{-}4$). Parameter k, however, corresponds to the thresholds in the data above the areal summation limit, A_{max}, while most of the data are for stimulus sizes below this value.

Contrast energy provides a useful metric for summarizing threshold performance with Gabor stimuli because it incorporates information from the full spatial–temporal profile of the stimulus rather than simply the peak contrast that represents the contrast of only a small number of high-contrast pixels (Watson, 2000; Watson & Ahumada, 2005; Watson, Barlow, & Robson, 1983). Contrast energy is defined as the integral over space and time of the square of the contrast waveform of a stimulus. For our data, the region to the left of A_{max} would appear flat if expressed in contrast energy units and the region to the right would rise with slope of 0.5. By transforming to contrast energy, then, we are able to test for differences in the region to the left of the summation limit. We transform the contrast thresholds to deciBarlows,[1] which are proportional to the stimulus detection efficiency (Watson, 2000), using the following equation:

$$dBB = 44.66 + 10 \log A_{max} + 20k. \quad (3)$$

Transforming the foveal thresholds to contrast energy by the above equation, we find that the difference with age is significant ($t = -3.958$, $df = 18$, $p = 9e - 4$). The average contrast energy values obtained (and 95% confidence intervals) were 17.94 (16.01, 19.94) for the younger observers and 24.34 (21.29, 27.47) for the older observers. As expected from previous investigations (Brown, Peierken, Bowman, & Crassini, 1989; Latham, Whitaker, & Wild, 1994; Werner et al., 2000), photopic increment thresholds are significantly elevated in older observers for foveal stimuli, but there is no significant change in spatial summation area with age.

Parafoveal spatial summation

The three-parameter and two-parameter models were fit to the parafoveal data using the same procedure as for the foveal data. The data of all but one (elderly) observer could be fit with these models. This observer was not included in the group comparisons because the nonlinear regression algorithm failed to estimate the parameters of the fit.[2]

Fourteen of 19 observers showed no significant difference in the model fits for a criterion of $p = 0.05$ (16 for $p = 0.01$) by a likelihood ratio test and 18 after adjusting for multiple testing by Bonferroni's correction. The parameter estimate and summary information from the fits of the 2-parameter model for each observer are shown in Table 4.

Fits of the two-parameter model to the parafoveal data of representative individuals are shown by the solid lines in Figure 4, and a fit based on the average parameters is shown in Figure 5. Arrows point to the spatial summation

Observer ID number	$\log_{10} A_{max}$	Standard error ($\log_{10} A_{max}$)	k	Standard error (k)	Residual SSE	Residual Standard error	Age (years)
S01	0.895	0.076	−1.005	0.03	0.379	0.138	21
S02	1.063	0.076	−1.44	0.03	0.056	0.053	21
S04	1.057	0.076	−1.586	0.03	0.069	0.059	21
S07	1.033	0.076	−1.454	0.03	0.361	0.134	21
S08	1.179	0.082	−1.282	0.035	0.3	0.122	23
S10	0.909	0.076	−1.376	0.03	0.14	0.084	21
S15	1.047	0.076	−1.552	0.03	0.062	0.056	21
S18	0.787	0.073	−1.384	0.027	0.097	0.07	21
S19	1.08	0.076	−1.328	0.03	0.195	0.099	10
S23	0.815	0.073	−1.563	0.027	0.065	0.057	20
S03	1.061	0.076	−1.194	0.03	0.077	0.062	74
S06	1.293	0.127	−1.384	0.06	0.14	0.084	67
S09	1.16	0.082	−1.304	0.035	0.099	0.07	70
S11	1.032	0.076	−1.415	0.03	0.089	0.067	67
S12	1.29	0.081	−0.956	0.035	0.094	0.065	83
S13	1.21	0.095	−1.513	0.043	0.161	0.09	68
S20	1.083	0.076	−1.224	0.03	0.095	0.069	80
S21	1.398	0.094	−1.624	0.043	0.16	0.085	83
S22	1.428	0.127	−1.319	0.06	0.168	0.092	72

Table 4. Summary of the fits of the 2-parameter model to the parafoveal data for each observer. Column 1: Observers' unique identification number. Column 2: $\log_{10} A_{max}$ estimate. Column 3: Standard error of $\log_{10} A_{max}$. Column 4: k estimate. Column 5: Standard error of k. Column 6: Residual sum of squared error. Column 7: Residual standard error of the fit. Column 8: Age of observers.

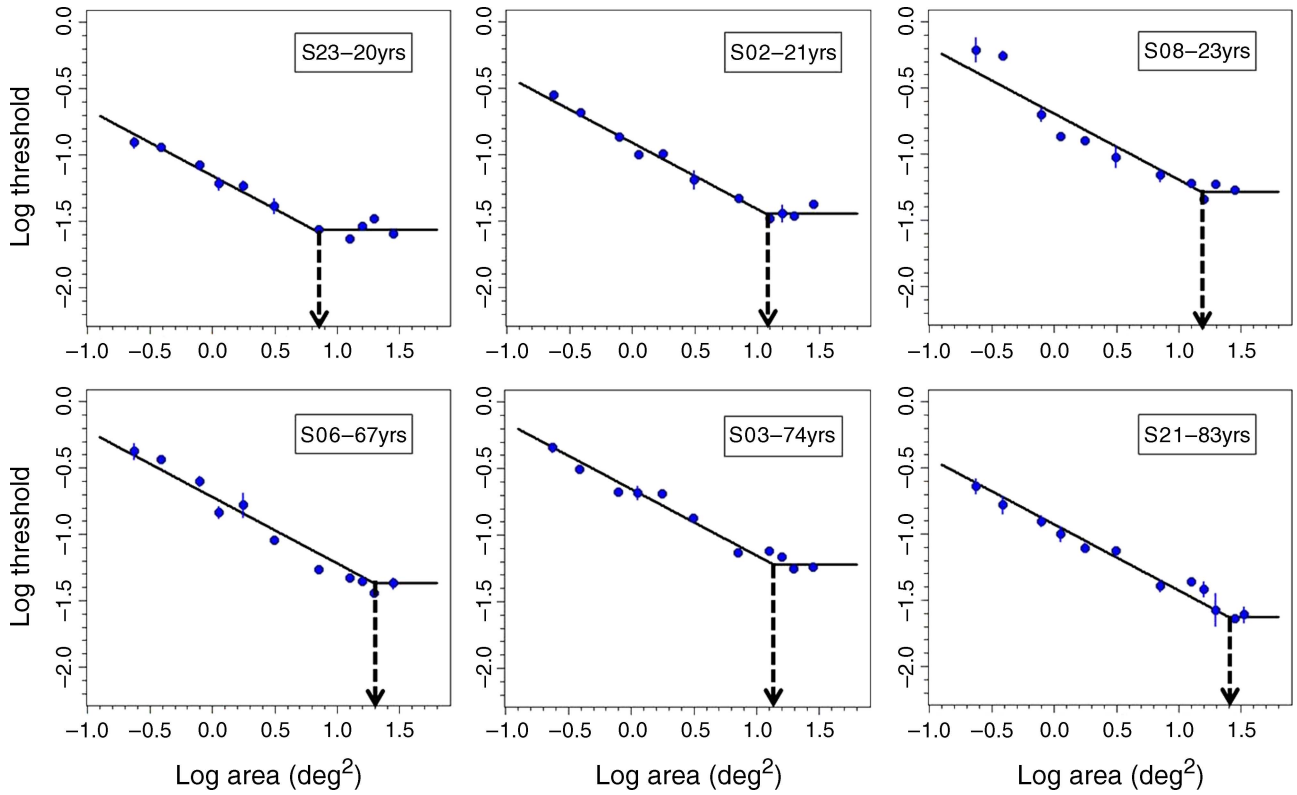

Figure 4. Log contrast detection thresholds (±1 *SEM*) at 6-deg nasal retina plotted as a function of log area. The identification code and the age of individual observers are shown in the upper right of each plot. The intersection of the two lines defines the spatial summation area indicated by the arrows.

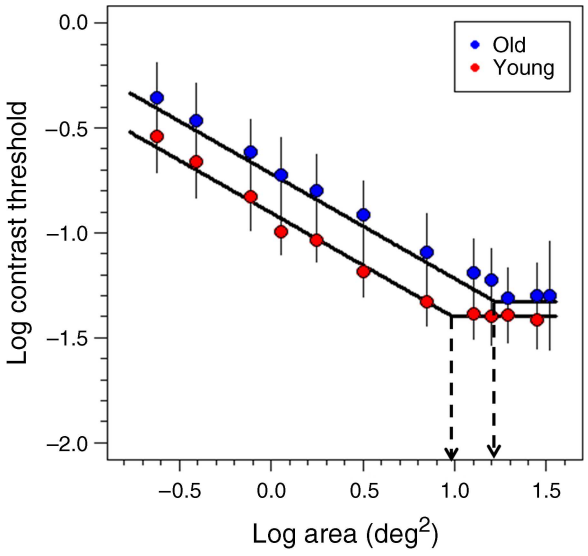

Figure 5. Parafoveal mean log contrast detection threshold as a function of stimulus area averaged across subjects plotted on a log–log scale. The error bars are 95% confidence intervals for interobserver differences. The model (Equation 2) fitted to the mean data was used for the best fitting curve.

areas defined by the intersection of the two-segmented function. The diameters correspond to 3.51 and 4.58 deg for the younger and older groups, respectively.

Contrary to the foveal data, age comparisons of the parameters using Student's *t*-tests indicate a significant difference in A_{max} ($t = -3.69$, $df = 17$, $p = 0.002$) but not in k ($t = -0.849$, $df = 17$, $p = 0.41$). These results demonstrate an age-related change in the area of maximal summation in the parafoveal data but not a change in sensitivity for the branch of the summation curve that shows independence. To test the branch below this region, we transformed the data to contrast energy. The results indicate a significant difference ($t = -2.189$, $df = 17$, $p = 0.043$) if we take significance as $p < 0.05$. The average contrast energy values (and 95% confidence intervals) are 26.59 (24.06, 29.19) for the younger observers and 30.31 (27.40, 33.31) for the older observers. The confidence intervals are based on the individual means and overlap, in apparent contradiction to the results from the *t*-test. The *t*-test, however, uses a pooled estimate of error, based on both samples, yielding a more sensitive indicator of the differences than that provided by the individual confidence intervals.

Discussion

The primary goal of these experiments was to examine age-related changes in spatial summation under photopic conditions. The results demonstrate significant differences in the size of the parafoveal (6-degree nasal retina) spatial summation area between younger and older observers but no significant age-related alteration of summation area in the fovea. In addition, peak contrast detection thresholds of older observers are significantly elevated for foveal stimuli with no significant difference between detection thresholds of younger and older observers in the parafovea. Expressed in terms of contrast energy, there was a significant elevation in threshold for elderly observers both in the fovea and in the parafovea. The energy thresholds reflect the height of the summation curve to the left of the maximal summation area. A shift of the maximal summation area with age suffices to produce a difference in thresholds in this region, even if the average heights of the functions do not change (see Figure 1).

The mean energy thresholds for younger and older observers in the fovea are 17.94 dBB and 24.34 dBB, respectively. Our subjects display higher energy thresholds than those of the Modelfest observers (~6 dBB for 4-cpd circular gratings in the fovea; see Figure 7 from Watson, 2000). Results from other studies that investigated spatial summation processes in an older population were transformed from contrast detection thresholds to energy thresholds for comparison with our results. In the parafovea, subjects from Redmond, Garway-Heath et al. (2010) displayed relatively higher energy thresholds (51.39 dBB and 56.59 dBB, respectively, for younger and older observers) than this study when thresholds were tested for achromatic stimuli at 10-deg eccentricity on the inferior visual field. Some of these differences may reflect differences in stimulus parameters, e.g., in the retinal illuminance or visual field eccentricity. Another source of variability between studies might result from observer experience, i.e., whether or not the subject is a naive or experienced psychophysical observer. Several studies have shown learning effects on contrast detection performance (De Valois, 1977; Mayer, 1983; Sowden, Rose, & Davies, 2002).

The two-branched model provided good fits to all our data but those of one observer. Some researchers, however, have suggested that the spatial summation curve has a more complex, multibranched shape and that each segment reflects different underlying mechanisms (e.g., Meese & Williams, 2000). The initial limb of the summation curve has a slope of −1 (Ricco's law) and is followed by a branch having a slope of −0.5 (Piper's law). This has been interpreted in terms of two mechanisms resulting from linear summation of signals and signal plus noise, respectively (Meese & Hess, 2007; Tyler & Chen, 2000). A branch of the summation curve, characterized by a slope of −0.25 (fourth-root rule), has been attributed to either probability summation among multiple filters (Meese & Williams, 2000; Quick, 1974; Robson & Graham, 1981; Sachs, Nachmias, & Robson, 1971; Tyler & Chen, 2000) or to nonlinear physiological summation (Cannon, 1995; Graham, 1989; Laming, 1988). After reaching a critical size, detection thresholds tend to asymptote to a constant value. This size-independent region has been interpreted in terms of the saturation of summation processes. To

examine a more complex model, the data were fitted with a three-branched curve having segments with slopes of −0.5, −0.25, and 0 using the following equation:

$$f(\log(A)) = 0.125(|\log(A) - \log(A_{ca})|) + 0.125(|\log(A) - \log(A_{max})|) - 0.25\log(A) + k + 0.125(A_{ca} + A_{max}), \quad (4)$$

where A is the stimulus area, A_{ca} is the critical summation area, which marks the cessation of Piper's law (intersection of branches with slopes of −0.5 and −0.25), and A_{max} is the maximal summation area, corresponding to the intersection of lines with slopes of −0.25 and 0. Because the tested stimulus areas are out of the range of the classically defined Ricco's area, we fitted the three-branched model to our data without an initial part (with slope = −1) of the summation curve. The two-branched model is nested within the three-branched model, so we could compare the fits by a likelihood ratio test For the foveal data, the difference in fits of the two models was not significant for 16/20 observers (20/20 after adjustment by Bonferroni's correction). For the parafoveal data, 15/19 of the data sets (17/19 after adjustment) showed no significant difference for the two models. Figure 6 shows a comparison of fits with two-branched and three-branched piece-wise linear models.

One possible interpretation for age-related changes in summation processes may be related to increased intrinsic neural noise in older observers as a result of age-related reduction of the efficiency of inhibitory processes (Betts, Sekuler, & Bennett, 2007; Leventhal, Wang, Pu, Zhou, & Ma, 2003; Schmolesky, Wang, Pu, & Leventhal, 2000). However, this hypothesis cannot explain the different effects of aging in the fovea and parafovea. Another explanation for differing results in these regions could be that human observers apply different detection algorithms for the two retinal loci. Manahilov, Simpson, and McCulloch (2001) argue that a cross-correlation algorithm is employed in detection of foveal stimuli, and an energy model might be used in detection of parafoveal or peripheral stimuli. Predictions of the energy model, which assumes the integration of squared filter outputs over spatial and temporal domains, would lead to a fitted log–log slope of the threshold improvement for peripheral stimuli of −0.5. We obtained very similar results for both foveal and parafoveal Gabor stimuli.

An alternative framework for our results is that they are due to neural plasticity in the adult visual system. Several authors proposed that the size of the summation area is defined by the inverse of ganglion cell density (Fischer, 1973; Garway-Heath, Caprioli, Fitzke, & Hitchings, 2000; Ransom-Hogg & Spillmann, 1980; Schefrin et al., 1998; Spillmann & Werner, 1996). There is strong evidence that ganglion cell density declines considerably with age (Curcio & Drucker, 1993; Harman et al., 2000; Morrison et al., 1990; Quigley et al., 1989). To maintain relatively stable visual perception across the life span, the visual system should compensate for age-related neural losses. One possible way to ameliorate losses in sensitivity associated with aging would be to reorganize neural networks by expansion of the cortical representation to maintain constant afferent inputs. Chino, Kaas, Smith, Langston, and Cheng (1992) found that following a small retinal lesion, substantial reorganization of cortical map-

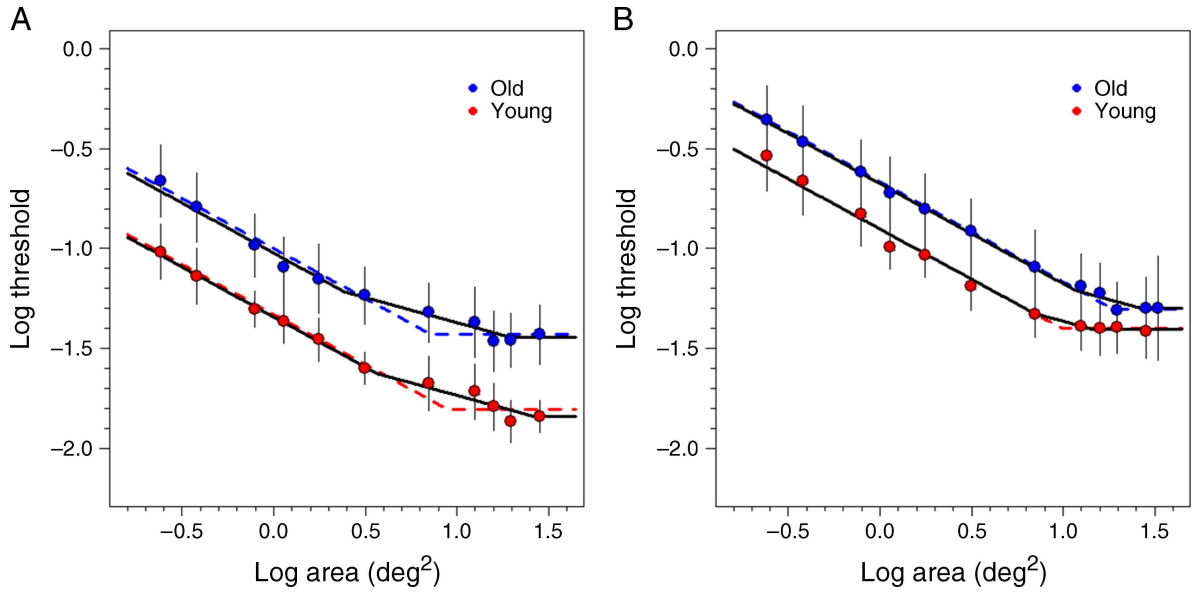

Figure 6. Mean contrast detection thresholds (±95% confidence intervals for interobserver differences) as a function of stimulus area at the (A) fovea and (B) parafovea. Black solid lines represent three-branched summation curve with slopes of −0.5, −0.25, and 0. Dashed red and blue lines are two-branched curves (slopes of −0.5 and 0) fitted to mean data of younger and older observers, respectively.

ping takes place in the visual cortex of adult cats. They suggested that adaptive modification in the effectiveness of existing connections plays a key role in the reorganization of cortical topography following peripheral deafferentation. In terms of spatial summation, neural plasticity should cause an enlargement of the summation area following neuronal loss in order to preserve sensitivity. Accordingly, we hypothesized that the plateau of parafoveal summation curves of elderly people would be shifted rightward toward larger stimuli. Indeed, Figure 5 shows that the summation area in the parafovea is increased by about 31%, while detection thresholds remained unchanged in older observers. The expansion of the spatial summation area is similar in magnitude to that reported by Schefrin et al. (1998) under scotopic conditions using a series of small spots imaged at the same retinal location. Surprisingly, no changes of summation area were found in elderly observers in the foveal region (see Figure 3). This region, however, sustains little age-related loss in cone photoreceptor density (Curcio et al., 1993).

Clinical studies support our hypothesis about the correlation between ganglion cell density and size of the spatial summation area. Glaucoma (Felius, Swanson, Fellman, Lynn, & Starita, 1997; Garway-Heath et al., 2000, Redmond, Zlatkova et al., 2010) and retinitis pigmentosa (Swanson, Felius, & Birch, 2000), both characterized by substantial losses of ganglion cells, showed increases in the spatial summation area relative to a normal control group, whereas patients with age-related macular degeneration, characterized primarily by outer retinal changes, exhibited unaltered summation areas along with substantial sensitivity losses (Zele, O'Loughlin, Guymer, & Vingrys, 2006). In all of these studies, generalizations depend on the severity and stage of disease at which measurements are made. Nevertheless, these results from patients are consistent with our earlier work on scotopic spatial summation (Schefrin et al, 1998) and present results on photopic spatial summation implying that losses in ganglion cells are compensated, at least in part, by expansion of the spatial summation area.

The results of this study invite analogies with findings of stability in color perception (Delahunt, Webster, Ma, & Werner, 2004; Hardy, Frederick, Kay, & Werner, 2005), chromatic sensitivity (Knoblauch, Vital-Durand, & Barbur, 2001; Werner & Steele, 1988), and orientation tuning mechanisms across the life span (Delahunt, Hardy, & Werner, 2008), which may also reflect continuous renormalization of networks to compensate neural losses that accompany normal aging processes.

Acknowledgments

This research was supported by the National Institute on Aging (Grant AG04058), U.S. Civilian Research and Development Foundation, and Research to Prevent Blindness. Frédéric Devinck was supported by grants from the Région Nord-Pas de Calais. We thank Reinhold Kliegl (University of Potsdam) for helpful comments.

Commercial relationships: none.
Corresponding author: Maka Malania.
Email: mmalania@mail.utexas.edu.
Address: 2617 Speedway, SW7, Room 104-105, Austin, TX 78712, USA.

Footnotes

[1]The deciBarlow (dBB), which is the logarithmic version of the Barlow unit, is a measure of the strength of a stimulus and is defined as dBB = 10logCE + 60. CE is the contrast energy of the stimulus and can be expressed as: CE = 0.394 * A_{max} * $(10^k)^2$. The leading coefficient is due to the reduction of contrast energy that results from counterphase modulation of the stimulus. If we combine these two equations and incorporate the spatial and temporal extent of the stimulus (presentation duration and the standard deviation of the Gaussian envelope) and a correction factor for the sinusoidal waveform, we obtain Equation 3 in the text.

[2]This observer's data did not show clear evidence of a transition to a horizontal independent branch and so the parameter estimates did not converge. One possibility is that A_{max} should be even higher in this observer.

References

Allen, M. J., & Vos, J. J. (1967). Ocular scattered light and visual performance as a function of age. *American Journal of Optometry and Physiological Optics, 44,* 717–727. [PubMed]

Artal, P., Ferro, M., Miranda, I., & Navarro, R. (1993). Effects of aging on retinal image quality. *Journal of the Optical Society of America A, Optics and Image Science, 10,* 1656–1662. [PubMed]

Barlow, H. B. (1958). Temporal and spatial summation in human vision at different background intensities. *The Journal of Physiology, 141,* 337–350. [PubMed]

Bates, D., Maechler, M., & Bolker, B. (2011). lme4: Linear mixed-effects models using S4 classes. R package version 0.999375-40/r1308. http://R-Forge.R-project.org/projects/lme4.

Betts, L. R., Sekuler, A. B., & Bennett, P. J. (2007). The effects of aging on orientation discrimination. *Vision Research, 47,* 1769–1780. [PubMed]

Brainard, D. H. (1997). The psychophysics toolbox. *Spatial Vision, 10,* 433–436. [PubMed]

Brainard, D. H., Pelli, D. G., & Robson, T. (2002). Display characterization. In J. P. Hornak (Ed.), *Encyclopedia of imaging science and technology* (pp. 72–188). New York: Wiley.

Brown, B., Peierken, C., Bowman, K., & Crassini, B. (1989). Spatial summation in young and elderly observers. *Ophthalmic and Physiological Optics, 9,* 310–313. [PubMed]

Cannon, M. W. (1995). A multiple spatial filter model for suprathreshold contrast perception. In E. Peli (Ed.), *Vision models for target detection and recognition* (pp. 88–116). London: World Scientific.

Chino, Y. M., Kaas, J. H., Smith, E. L., Langston, A. L., & Cheng, H. (1992). Rapid reorganization of cortical maps in adult cats following restricted deafferentation in retina. *Vision Research, 32,* 789–796. [PubMed]

Cohn, T. E. (1990). Spatial and temporal summation in human vision. In C. Blakemore (Ed.), *Vision: Coding and efficiency* (pp. 376–385). Cambridge, UK: Cambridge University Press.

Curcio, C. A., & Allen, K. A. (1990). Topography of ganglion cells in human retina. *Journal of Comparative Neurology, 300,* 5–25. [PubMed]

Curcio, C. A., & Drucker, D. N. (1993). Retinal ganglion cells in Alzheimer's disease and aging. *Annals of Neurology, 33,* 248–257. [PubMed]

Curcio, C. A., Medeiros, N. E., & Millican, C. L. (1998). The Alabama age-related macular degeneration grading system for donor eyes. *Investigative Ophthalmology & Visual Science, 39,* 1085–1096. [PubMed]

Curcio, C. A., Millican, C. L., Allen, K. A., & Kalina, R. E. (1993). Aging of the human photoreceptor mosaic: Evidence for selective vulnerability of rods in central retina. *Investigative Ophthalmology & Visual Science, 34,* 3278–3296. [PubMed]

Daugman, J. G. (1985). Uncertainty relation for resolution in space, spatial frequency, and orientation optimized by two-dimensional visual cortical filters. *Journal of the Optical Society of America A, Optics and Image Science, 2,* 1160–1169. [PubMed]

Davila, K. D., & Geisler, W. S. (1991). The relative contributions of pre-neural and neural factors to areal summation in the fovea. *Vision Research, 31,* 1369–1380. [PubMed]

Delahunt, P. B., Hardy, J. L., & Werner, J. S. (2008). The effect of senescence on orientation discrimination and mechanism tuning. *Journal of Vision, 8*(3):5, 1–9, http://www.journalofvision.org/content/8/3/5, doi:10.1167/8.3.5. [PubMed] [Article]

Delahunt, P. B., Webster, M. A., Ma, L., & Werner, J. S. (2004). Long-term renormalization of chromatic mechanisms following cataract surgery. *Visual Neuroscience, 21,* 301–307. [PubMed]

De Valois, K. K. (1977). Spatial frequency adaptation can enhance contrast sensitivity. *Vision Research, 17,* 1057–1065. [PubMed]

Felius, J., Swanson, W. H., Fellman, R. L., Lynn, J. R., & Starita, R. J. (1997). Spatial summation for selected ganglion cell mosaics in patients with glaucoma. In M. Wall & A. Heijl (Eds.), *Perimetry update 1996/1997* (pp. 213–221). Amsterdam, The Netherlands: Kugler Publications.

Fischer, B. (1973). Overlap of receptive field centers and representation of the visual field in the cat's optic tract. *Vision Research, 13,* 2113–2120. [PubMed]

Garway-Heath, D. F., Caprioli, J., Fitzke, F. W., & Hitchings, R. A. (2000). Scaling the hill of vision: The physiological relationship between light sensitivity and ganglion cell numbers. *Investigative Ophthalmology & Visual Science, 41,* 1774–1782. [PubMed]

Gilbert, C. D., & Wiesel, T. N. (1992). Receptive field dynamics in adult primary visual cortex. *Nature, 356,* 150–152. [PubMed]

Glezer, V. D. (1965). The receptive fields of the retina. *Vision Research, 5,* 497–525. [PubMed]

Graham, C. H., & Margaria, R. (1935). Area and the intensity time relation in peripheral retina. *American Journal of Physiology, 113,* 299–305.

Graham, N., Robson, J. G., & Nachmias, J. (1978). Grating summation in fovea and periphery. *Vision Research, 18,* 815–825. [PubMed]

Graham, N. V. S. (1989). *Visual pattern analyzers*. New York: Oxford University Press.

Hardy, J. L., Frederick, C. M., Kay, P., & Werner, J. S. (2005). Color naming, lens aging, and grue. *Psychological Science, 16,* 321–327. [PubMed]

Harman, A., Abrahams, B., Moore, S., & Hoskins, R. (2000). Neuronal density in the human retinal ganglion cell layer from 16–77 years. *The Anatomical Record, 260,* 124–131. [PubMed]

Hoekstra, J., van der Goot, D. P., van den Brink, G., & Bilsen, F. A. (1974). The influence of the number of cycles upon the visual contrast threshold for spatial sine wave patterns. *Vision Research, 14,* 365–368. [PubMed]

Howell, E. R., & Hess, R. F. (1978). The functional area for summation to threshold for sinusoidal gratings. *Vision Research, 18,* 369–374. [PubMed]

Inui, T., Mimura, O., & Kani, K. (1981). Retinal sensitivity and spatial summation in the foveal and parafoveal regions. *Journal of the Optical Society of America, 71,* 151–163. [PubMed]

Jackson, G. R., & Owsley, C. (2000). Scotopic sensitivity during adulthood. *Vision Research, 40,* 2467–2473. [PubMed]

Jones, J. P., & Palmer, L. A. (1987). An evaluation of the two-dimensional Gabor filter model of simple receptive fields in cat striate cortex. *Journal of Neurophysiology, 58,* 1233–1258. [PubMed]

Knoblauch, K., Vital-Durand, F., & Barbur, J. (2001). Variation of chromatic sensitivity across the life span. *Vision Research, 41,* 23–36. [PubMed]

Laming, D. (1988). Precis of sensory analysis. *Behavioural and Brain Sciences, 11,* 275–339.

Latham, K., Whitaker, D., & Wild, J. M. (1994). Spatial summation of the differential light threshold as a function of visual field location and age. *Ophthalmic & Physiological Optics, 14,* 71–78. [PubMed]

Lennie, P., & Fairchild, M. D. (1994). Ganglion cell pathways for rod vision. *Vision Research, 34,* 477–482. [PubMed]

Leventhal, A. G., Wang, Y. C., Pu, M. L., Zhou, Y. F., & Ma, Y. Y. (2003). GABA and its agonists improved visual cortical function in senescent monkeys. *Science, 300,* 812–815. [PubMed]

Li, Z.-Y., Kljavin, I. J., & Milam, A. H. (1995). Rod photoreceptor neurite sprouting in retinitis pigmentosa. *Journal of Neuroscience, 15,* 5429–5438. [PubMed]

Liang, J., & Westheimer, G. (1995). Optical performance of human eyes derived from double-pass measurements. *Journal of the Optical Society of America A, Optics, Image Science, and Vision, 12,* 1411–1416. [PubMed]

Lie, I. (1980). Visual detection and resolution as a function of retinal eccentricity. *Vision Research, 20,* 967–974. [PubMed]

Manahilov, V., Simpson, W. A., & McCulloch, D. L. (2001). Spatial summation of peripheral Gabor patches. *Journal of the Optical Society of America A, Optics, Image Science, and Vision, 18,* 273–282. [PubMed]

Marcelja, S. (1980). Mathematical description of the responses of simple cortical cells. *Journal of the Optical Society of America, 70,* 1297–1300. [PubMed]

Mayer, M. (1983). Practice improves adults' sensitivity to diagonals. *Vision Research, 23,* 547–550. [PubMed]

Meese, T. S., & Hess, R. F. (2007). Anisotropy for spatial summation of elongated patches of grating: A tale of two tails. *Vision Research, 47,* 1880–1892. [PubMed]

Meese, T. S., & Williams, C. B. (2000). Probability summation for multiple patches of luminance modulation. *Vision Research, 40,* 2101–2113. [PubMed]

Merzenich, M. M., Nelson, R. J., Stryker, M. P., Cynader, M. S., Schoppmann, A., & Zook, J. M. (1984). Somatosensory cortical map changes following digit amputation in adult monkeys. *Journal of Comparative Neurology, 224,* 591–605. [PubMed]

Milam, A. H., Li, Z.-Y., & Fariss, R. N. (1998). Histopathology of the human retina in retinitis pigmentosa. *Progress in Retinal Eye Research, 17,* 175–205. [PubMed]

Morrison, J. C., Cork, L. C., Dunkelberger, G. R., Brown, A., & Quigley, H. A. (1990). Aging changes of the rhesus monkey optic nerve. *Investigative Ophthalmology & Visual Science, 31,* 1623–1627. [PubMed]

Panda-Jonas, S., Jonas, J. B., & Jakobczyk-Zmija, M. (1995). Retinal photoreceptor density decreases with age. *Ophthalmology, 102,* 1853–1859. [PubMed]

Pelli, D. G. (1997). The VideoToolbox software for visual psychophysics: Transforming numbers into movies. *Spatial Vision, 10,* 437–442. [PubMed]

Pinheiro, J. C., & Bates, D. M. (2000). *Mixed-effects models in S and S-PLUS*. New York: Springer.

Piper, H. (1903). Uber die abhangigkeit des reizwertes leuchtender objekte von ihrer flachen-bezsw. Winkelgrosse. *Zeitschrift fur Psychologie und Physiologie der Sinnesorgane, 32,* 98–112.

Quick, R. F. (1974). A vector magnitude model of contrast detection. *Kybernetic, 16,* 65–67. [PubMed]

Quigley, H. A., Dunkelberger, G. R., & Green, W. R. (1989). Retinal ganglion cell atrophy correlated with automated perimetry in human eyes with glaucoma. *American Journal of Ophthalmology, 107,* 453–464. [PubMed]

R Development Core Team (2010). *R: A Language and Environment for Statistical Computing*. Vienna, Austria: R Foundation for Statistical Computing. http://www.R-project.org.

Ransom-Hogg, A., & Spillmann, L. (1980). Perceptive field size in fovea and periphery of the light- and dark-adapted retina. *Vision Research, 20,* 221–228. [PubMed]

Redmond, T., Garway-Heath, D. F., Zlatkova, M. B., & Anderson, R. S. (2010). Sensitivity loss in early glaucoma can be mapped to an enlargement of the area of complete spatial summation. *Investigative Ophthalmology & Visual Science, 51,* 6540–6548. [PubMed]

Redmond, T., Zlatkova, M. B., Garway-Heath, D. F., & Anderson, R. S. (2010). The effect of age on the area of complete spatial summation for chromatic and achromatic stimuli. *Investigative Ophthalmology & Visual Science, 51,* 6533–6539. [PubMed]

Ricco, A. (1877). Relazione fra il minimo angolo visuale e l'intensita' luminosa. *Memorie della Regia Accademia di Scienze, Lettere ed Arti in Modena, 17,* 47–160.

Richards, W. (1967). Apparent modifiability of receptive fields during accommodation and convergence and a model for size constancy. *Neuropsychologia, 5,* 63–72.

Ringach, D. L. (2002). Spatial structure and symmetry of simple-cell receptive fields in macaque primary visual cortex. *Journal of Neurophysiology, 88,* 455–463. [PubMed]

Robson, J. G., & Graham, N. (1981). Probability summation and regional variation in contrast sensitivity across the visual field. *Vision Research, 21,* 409–418. [PubMed]

Rovamo, J., Luntinen, O., & Näsänen, R. (1993). Modeling the dependence of contrast sensitivity on grating area and spatial frequency. *Vision Research, 33,* 2773–2788. [PubMed]

Rovamo, J., Virsu, V., & Näsänen, R. (1978). Cortical magnification factor predicts the photopic contrast sensitivity of peripheral vision. *Nature, 271,* 54–56. [PubMed]

Sachs, M. B., Nachmias, J., & Robson, J. G. (1971). Spatial frequency channels in human vision. *Journal of the Optical Society of America, 61,* 1176–1186. [PubMed]

Sakitt, B. (1971). Configuration dependence of scotopic spatial summation. *The Journal of Physiology, 216,* 513–529. [PubMed]

Savoy, R. L., & McCann, J. J. (1975). Visibility of low spatial-frequency sine-wave targets: Dependence on number of cycles. *Journal of the Optical Society of America, 65,* 343–350. [PubMed]

Schefrin, B. E., Bieber, M. L., McLean, R., & Werner, J. S. (1998). The area of complete scotopic spatial summation enlarges with age. *Journal of the Optical Society of America A, Optics, Image Science, and Vision, 15,* 340–348. [PubMed]

Schefrin, B. E., Hauser, M., & Werner, J. S. (2004). Evidence against age-related enlargements of ganglion cell receptive field centers under scotopic conditions. *Vision Research, 44,* 423–428. [PubMed]

Schefrin, B. E., Tregear, S. J., Harvey, L. O., Jr., & Werner, J. S. (1999). Senescent changes in scotopic contrast sensitivity. *Vision Research, 39,* 3728–3736. [PubMed]

Schmolesky, M. T., Wang, Y., Pu, M., & Leventhal, A. G. (2000). Degradation of stimulus selectivity of visual cortical cells in senescent rhesus monkeys. *Nature Neuroscience, 3,* 384–390. [PubMed]

Scholtes, A. M. W., & Bouman, M. A. (1977). Psychophysical experiments on spatial summation at threshold level of the human peripheral retina. *Vision Research, 17,* 867–873. [PubMed]

Sowden, P. T., Rose, D., & Davies, I. R. L. (2002). Perceptual learning of luminance contrast detection: Specific for spatial frequency and retinal location but not orientation. *Vision Research, 42,* 1249–1258. [PubMed]

Spear, P. D. (1993). Neural bases of visual deficits during aging. *Vision Research, 33,* 2589–2609. [PubMed]

Spillmann, L., & Werner, J. S. (1996). Long-range interactions in visual perception. *Trends in Neurosciences, 19,* 428–434. [PubMed]

Swanson, W. H., Felius, J., & Birch, D. G. (2000). Effect of stimulus size on static visual fields in patients with retinitis pigmentosa. *Ophthalmology, 107,* 1950–1954. [PubMed]

Thibos, L. N. (1998). Acuity perimetry and the sampling theory of visual resolution. *Optometry & Vision Science, 75,* 399–406. [PubMed]

Tyler, C. W., & Chen, C. C. (2000). Signal detection theory in the 2AFC paradigm: Attention, channel uncertainty and probability summation. *Vision Research, 40,* 3121–3144. [PubMed]

van der Kraats, J., & van Norren, D. (2007). Optical density of the aging human ocular media in the visible and the UV. *Journal of the Optical Society of America A, Optics, Image Science, and Vision, 24,* 1842–1857. [PubMed]

Volbrecht, V. J., Shrago, E. E., Schefrin, B. E., & Werner, J. S. (2000). Spatial summation in human cone mechanisms from 0° to 20° in the superior retina. *Journal of the Optical Society of America A, Optics, Image Science, and Vision, 17,* 641–650. [PubMed]

Watson, A. B. (2000). Visual detection of spatial contrast patterns: Evaluation of five simple models. *Optics Express, 6,* 12–33. [PubMed]

Watson, A. B., & Ahumada, A. J., Jr. (2005). A standard model for foveal detection of spatial contrast. *Journal of Vision, 5*(9):6, 717–740, http://www.journalofvision.org/content/5/9/6, doi:10.1167/5.9.6. [PubMed] [Article]

Watson, A. B., Barlow, H. B., & Robson, J. G. (1983). What does the eye see best? *Nature, 302,* 419–422. [PubMed]

Watson, A. B., & Pelli, D. G. (1983). Quest: A Bayesian adaptive psychometric method. *Perception & Psychophysics, 33,* 113–120. [PubMed]

Weale, R. A. (1988). Age and the transmittance of the human crystalline lens. *The Journal of Physiology, 395,* 577–587. [PubMed]

Werner, J. S., Schefrin, B. E., & Bieber, M. L. (2000). Senescence of foveal and parafoveal cone sensitivities and their relations to macular pigment density. *Journal of the Optical Society of America A, Optics, Image Science, and Vision, 17,* 1918–1932. [PubMed]

Werner, J. S., Schefrin, B. E., & Bradley, A. (2010). Optics and vision of the aging eye. In M. Bass, J. M. Enoch, E. W. VanStryland, & W. L. Wolfe (Eds.), *OSA handbook of optics: Classical, Vision & X-ray*

Optics (vol. 3, pp. 13.1–13.31). New York: McGraw Hill.

Werner, J. S., Schelble, K. A., & Bieber, M. L. (2001). Age-related increases in photopic increment thresholds are not due to an elevation in intrinsic noise. *Color Research and Application, 26,* 48–52. [PubMed]

Werner, J. S., & Steele, V. G. (1988). Sensitivity of human foveal color mechanisms throughout the life span. *Journal of the Optical Society of America A, Optics, Image Science, and Vision, 5,* 2122–2130. [PubMed]

Wilson, M. E. (1970). Invariant features of spatial summation with changing locus in the visual field. *The Journal of Physiology, 207,* 611–622. [PubMed]

Winn, B., Whitaker, D., Elliott, D. B., & Phillips, N. J. (1994). Factors affecting light adapted pupil size in normal human subjects. *Investigative Ophthalmology & Visual Science, 35,* 1132–1137. [PubMed]

Wolf, E., & Gardner, J. S. (1965). Studies on the scatter of light in the dioptric media of the eye as a basis of visual glare. *Archives of Ophthalmology, 74,* 338–345. [PubMed] [Article]

Zele, A. J., O'Loughlin, R. K., Guymer, R. H., & Vingrys, A. J. (2006). Disclosing disease mechanisms with a spatio-temporal summation paradigm. *Graefe's Archive for Clinical and Experimental Ophthalmology, 244,* 425–432. [PubMed]